On the Origin of Tunneling Currents in Scaled Silicon Devices

A. Schenk, U. Krumbein, S. Müller, H. Dettmer, and W. Fichtner

Swiss Federal Institute of Technology, Integrated Systems Laboratory,
Gloriastrasse 35, CH-8092 Zürich, Switzerland

In recent years tunneling generation has been found to be a source of leakage in advanced silicon devices. Forward bias tunneling in the emitter-base junction of bipolar transistors [1], gate-induced drain and trench-gated diode leakage in DRAM cells [2], gate-induced drain leakage in MOSFETs [3] and device degradation due to tunneling-created carriers [4] are well known examples. Besides, tunneling generation is intentionally used for (band-to-band) tunneling induced substrate hot-electron injection (BBISHE) in non-volatile memories [5].

In most cases band-to-band tunneling (BBT) has been assumed for the generation process. By measuring the drain current of MOSFETs BBT was inferred from the $\ln[I_D/(V_{DG} - 1.2)]$ versus $1/(V_{DG} - 1.2)$ dependence [3,4] showing basically a constant slope. However, a similar behaviour is also to be expected from trap-assisted tunneling (TAT). It is not possible to extract a "critical" field strength from the cumbersome field dependence of TAT, but numerical calculations [6,7] gave comparable slopes at least for the more weakly coupled recombination centers. As another proof whether TAT or BBT is responsible for the above mentioned effects the temperature dependence of $I - V$ characteristics has been used [3]. It is generally assumed that TAT has a much stronger temperature effect than BBT because of the Shockley-Read-Hall (SRH) statistics and the temperature dependence of the capture cross sections. However, the field-enhancement factors of SRH lifetimes exhibit a contrary temperature effect leading to a compensation of the T–dependence of the intrinsic density n_i in the tunneling regime [6].

In this paper we study the relative influence of TAT and BBT in tunneling generation by numerical simulation. Microscopic models of TAT [6] (field-enhanced multiphonon recombination) and phonon-assisted BBT [7] were implemented into the device simulator **SIMUL** [8]. The investigated structure is a $n^+ - p$ diode. The n^+ doping has an error function profile with a surface concentration of $N_D = 10^{20} \, cm^{-3}$ and a junction depth of 140 nm. The bulk concentration is variing from $N_A = 10^{17} \, cm^{-3}$ to $10^{19} \, cm^{-3}$. Such a structure is relevant for advanced bipolar devices and the MOS-gated diode. The conclusions are less applicable to BBISHE where confined states modify the tunneling probability (not modeled in **SIMUL**). In addition models of the following physical effects were used, all described in [8]: temperature-dependent bandgap, bandgap narrowing, doping and field dependent mobilities, avalanche generation (local field version), Auger recombination (band-to-band and trap-assisted), and doping dependence of SRH lifetimes.

Fig. 1 shows reverse $I - V$ characteristics of the individual generation-recombination processes ("SRH+Au" - Auger and SRH recombination without field enhancement, "Ava" - Avalanche generation) and the resulting curve (all) for a $1 \, \mu m \times 1 \, \mu m$ diode and N_A-concentrations ranging from $10^{17} \, cm^{-3}$ to $10^{18} \, cm^{-3}$. Here the doping dependence of the SRH lifetimes (Scharfetter relation) was suppressed in order to obtain a lower limit for TAT. A midgap level and $0.240 \, eV$ for the lattice relaxation energy ϵ_R of the recombination center were used. The influence of BBT increases as the junctions become steeper, but TAT dominates the pre-breakdown up to $-4 \, V$. Impact ionization remains unimportant because the junctions are too narrow.

Effects in the forward characteristic are only observed if the p- concentration is further increased (Fig. 2). In the case $N_A = 10^{19} \, cm^{-3}$ the forward bias tunneling is still merely determined by TAT.

To obtain a possible lower limit of TAT, the lattice relaxation energy ϵ_R was varied in Fig. 3 from $0.4 \, eV$ (strong coupling) to $0.05 \, eV$ (weak coupling). Strongly coupled centers exhibit the lowest TAT, but the pre-breakdown remains in any case dominated by TAT up to the onset of BBT. The slope increases with decreasing coupling strength and becomes similar to that of BBT for $\epsilon_R \approx 0.1 \, eV$. If one assumes the strongest coupled recombination centers to determine the zero field SRH lifetimes, and if one further assumes that other centers with a smaller coupling strength (and therefore with larger SRH lifetimes and a steeper slope) come into play at higher voltages, the TAT characteristic becomes a superposition of these curves. Therefore, from a $\ln[I_D/(V - 1.2)]$ versus $1/(V - 1.2)$ dependence one cannot unambiguously distinguish between BBT and TAT.

Fig. 4 shows the simulated temperature dependence of BBT and TAT together with SRH+Au. Before tunneling sets in, the difference is mainly due to n_i. In the BBT regime (Fig. 4a) higher temperatures increase the current because of the shrinked bandgap and the larger phonon occupation. In the case of TAT (Fig. 4b) the field enhancement factors increase the lifetimes with rising temperature and compensate the strong temperature effect from n_i – the more the lower the temperature. At higher field strengths the temperature difference of $I - V$ curves in the TAT regime is largly reduced. For the zero field lifetimes a T^2-law was used. Thus, even the temperature dependence is not the strong criterion to decide wether BBT or TAT dominates the $I - V$ characteristics.

In conclusion, our results indicate that the field and temperature dependences of TAT may be similar to those of BBT. The low-voltage range of $I - V$ characteristics of $n^+ - p$ junctions is determined by TAT. If a model for the doping dependence of SRH lifetimes is used in the simulation, the dominance of TAT in the pre-breakdown range further increases.
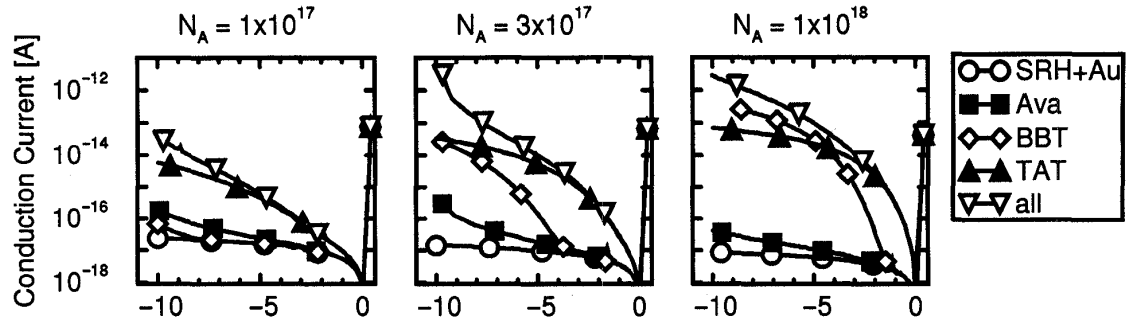
Fig. 1: Reverse I–V characteristics with different generation–recombination processes (T=300K, TAT: $\epsilon_R = 240$ meV).

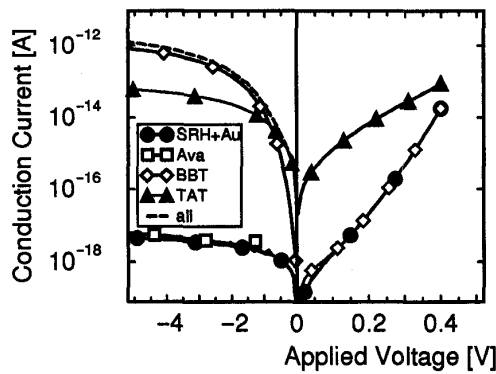Figure 2: I–V characteristics of a p–n junction with $N_A = 10^{19} cm^{-3}$ and $N_D = 10^{20} cm^{-3}$ (T=300K, $\epsilon_R = 240$ meV).
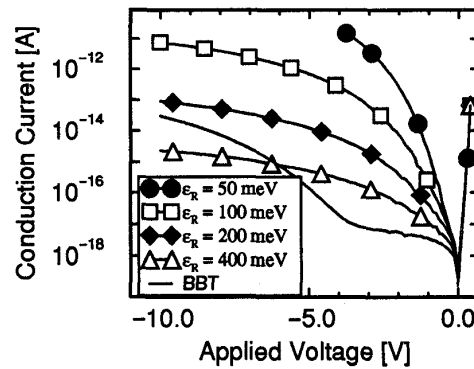

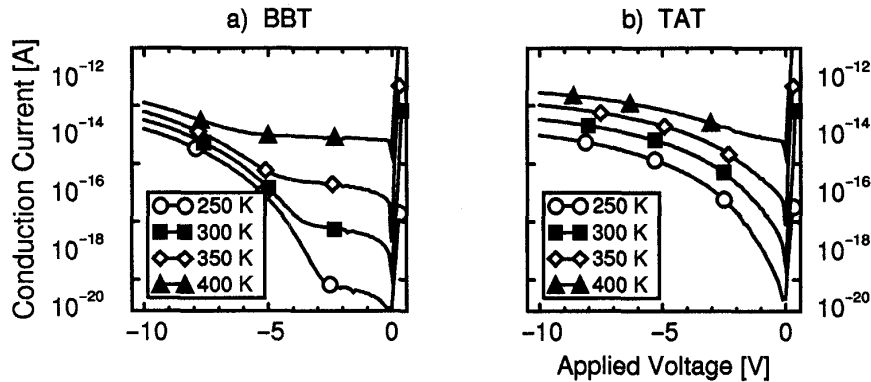Figure 3: I–V characteristics for different lattice relaxation energies (T=300K, $N_A = 3 \cdot 10^{17} cm^{-3}$).

Figure 4: a) BBT and b) TAT with $N_A = 3 \cdot 10^{17} cm^{-3}$, $\epsilon_R = 240$ meV at different temperatures.

[1] J. del Alamo and R. M. Swanson, IEEE Electron Device Letters **7** (11), 629 (1986)

[2] S. H. Voldman, J. B. Johnson, T. D. Linton, and S. L. Titcomb, IEDM Tech. Digest, p. 349 (1990)

[3] T. Y. Chan, J. Chen, P. K. Ko, and C. Hu, IEDM Tech. Digest, p. 718 (1987)

[4] Y. Igura, H. Matsuoka, and E. Takeda, IEEE Electron Device Letters **10** (7), 227 (1989)

[5] I.-C. Chen, D. J. Coleman, and C. W. Teng, IEEE Electron Device Letters **10** (7), 297 (1989)

[6] A. Schenk, Solid-State Electronics **35** (11), 1585 (1992)

[7] A. Schenk, Solid-State Electronics **36** (1), 19 (1993)

[8] **SIMUL** Manual, IIS, ETH Zürich, Switzerland, 1.0 (alpha) edition (1992)